AGU PUBLICATIONS

Geophysical Research Letters

RESEARCH LETTER
10.1002/2014GL060197

Key Points:
- The postmonsoon Bay of Bengal tropical cyclones increased in intensity
- Changes in several oceanic and atmospheric parameters are responsible
- These environmental changes are part of long-term trends

Supporting Information:
- Readme
- Text S1
- Figure S1
- Figure S2
- Figure S3
- Figure S4

Correspondence to:
K. Balaguru,
Karthik.Balaguru@pnnl.gov

Citation:
Balaguru, K., S. Taraphdar, L. R. Leung, and G. R. Foltz (2014), Increase in the intensity of postmonsoon Bay of Bengal tropical cyclones, *Geophys. Res. Lett.*, *41*, 3594–3601, doi:10.1002/2014GL060197.

Received 14 APR 2014
Accepted 6 MAY 2014
Accepted article online 10 MAY 2014
Published online 29 MAY 2014

Increase in the intensity of postmonsoon Bay of Bengal tropical cyclones

Karthik Balaguru[1], Sourav Taraphdar[1], L. Ruby Leung[1], and Gregory R. Foltz[2]

[1]Atmospheric Sciences and Global Change, Pacific Northwest National Laboratory, Richland, Washington, USA, [2]Physical Oceanography Division, Atlantic Oceanographic and Meteorological Laboratory, Miami, Florida, USA

Abstract The postmonsoon (October–November) tropical cyclone (TC) season in the Bay of Bengal (BoB) has spawned many of the deadliest storms in recorded history. Here it is shown that the intensity of major TCs (wind speed > 49 m s^{-1}) in the postmonsoon BoB increased during 1981–2010. It is found that changes in environmental parameters are responsible for the observed increases in TC intensity. Increases in sea surface temperature and upper ocean heat content made the ocean more conducive to TC intensification, while enhanced convective instability made the atmosphere more favorable for the growth of TCs. The largest changes in the atmosphere and ocean occurred in the eastern BoB, where nearly all major TCs form. These changes are part of positive linear trends, suggesting that the intensity of postmonsoon BoB TCs may continue to increase in the future.

1. Introduction

The Bay of Bengal (BoB) is marginally conducive to tropical cyclone (TC) formation, with an average of three to four storms annually [*Alam et al.*, 2003]. Despite lower TC formation rates in the BoB compared to the Atlantic and Pacific basins, a combination of factors, such as shallow bathymetry, low-lying and flat coastal terrain, and high-population density of surrounding countries, often leads to devastating consequences when TCs make landfall [*Webster*, 2008; *Islam and Peterson*, 2009; *McPhaden et al.*, 2009; *Lin et al.*, 2009]. Since the BoB is a semienclosed basin, most of the TCs that form make landfall, giving BoB TCs a disproportionately high societal importance relative to their small total number.

There are two primary TC seasons in the northern Indian Ocean: the premonsoon season during April–May and the more active postmonsoon season during October–November [*Girishkumar and Ravichandran*, 2012]. This bimodal structure of the TC season in the northern Indian Ocean owes its existence to the strong vertical wind shear during the summer monsoon months of June–September [*Hoarau et al.*, 2012]. Eight of the 13 strongest TCs in the BoB since 1970 formed during the postmonsoon period (October–November) (http://www.imd.gov.in/section/nhac/dynamic/faq/FAQP.htm). More recently, cyclone Phailin made landfall in India in October 2013, prompting the evacuation of 500,000 people. Along with a thermodynamically unstable atmosphere and weak tropospheric vertical wind shear, favorable hydrographic conditions, such as the formation of thick barrier layers that stably stratify the upper ocean, are the primary reasons for enhanced TC activity during the postmonsoon season [*McPhaden et al.*, 2009; *Sengupta et al.*, 2008]. The freshwater discharge from the Ganges, Brahmaputra, and Irrawaddy river systems cause the uniform density mixed layers to become shallower than the uniform temperature isothermal layers due to the salinity effect, leading to the formation of salt-stratified barrier layers in the BoB [*Sprintall and Tomczak*, 1992]. Once formed, the salinity stratification acts as a "barrier" to vertical mixing and entrainment cooling induced by TCs, leading to an increase in enthalpy flux from the ocean into the atmosphere and, consequently, an invigoration of TCs [*Balaguru et al.*, 2012].

A few previous studies investigated the interannual variability of postmonsoon BoB TC activity, focusing on climate phenomena such as El Niño Southern Oscillation [*Girishkumar and Ravichandran*, 2012; *Ng and Chan*, 2012], Indian Ocean Dipole [*Singh*, 2008; *Girishkumar and Ravichandran*, 2012], and the Madden-Julian Oscillation [*Kikuchi and Wang*, 2010; *Girishkumar and Ravichandran*, 2012], and several studies examined changes in TC activity in a warming world. *Knutson and Tuleya* [2004] showed consistent CO_2-induced increases in TC intensity in coupled climate models but considered only the Atlantic and Pacific basins. *Emanuel* [2005] found significant increases in the power dissipated by TCs in the Atlantic and Pacific since 1970 but did not

examine changes in the Indian Ocean. *Webster et al.* [2005] showed consistent increases in the number and percentage of intense TCs across all basins since 1970. However, they grouped all North Indian Ocean storms together so that changes in BoB cyclone intensity could not be discerned from those in the Arabian Sea. *Elsner et al.* [2008] concluded that there has been an increase in the intensities of the strongest TCs, though they did not address BoB cyclone activity specifically.

Analyses of TC trends in the BoB have been more limited. *Singh et al.* [2001] evaluated trends in postmonsoon BoB TC activity for the 122 year period 1877–1998 and concluded that both TC frequency and intensity increased in the month of November. However, the reasons for the observed trends were not identified, and TC track data before the advent of satellites may not be reliable [*Klotzbach*, 2006]. In this study, we examine changes in TC activity over the 30 year satellite period (1981–2010) and identify their possible causes. The availability of various satellite and reanalysis data for this period also allows us to examine the evolution of environmental parameters that are likely to influence TC development.

2. Data and Methods

Several different data sets are used in this study. TC track data for the 30 year period 1981–2010, obtained from http://eaps4.mit.edu/faculty/Emanuel/ [*Emanuel*, 2005], are used to calculate the TC power dissipation index (PDI) and the intensification tendencies. The PDI for a season and for a given TC strength category (tropical storm, tropical cyclone, major tropical cyclone) is estimated as the sum of the cubes of the maximum wind speed at each 6-hourly TC location during the months of October–November, wherever the maximum wind speed of the storm is within the range defined for that category [*Emanuel*, 2005]. The intensification tendency for a storm at a location is estimated as the linear regression coefficient of the maximum wind speed over the current and five subsequent 6-hourly snapshots [*Lloyd and Vecchi*, 2011].

Observed monthly mean sea surface temperature (SST) data, obtained from the UK Met Office Hadley Center (http://www.metoffice.gov.uk/hadobs/hadisst/) [*Rayner et al.*, 2003] for the period 1981–2010 and from NOAA (http://www.esrl.noaa.gov/psd/data/) [*Reynolds et al.*, 2002] for the period 1982–2010 are used to evaluate changes and trends in SST. Here we define changes as the October–November 1996–2010 mean minus the October–November 1981–1995 mean. Monthly mean oceanic temperature data, obtained from two different products for the period 1981–2010—Geophysical Fluid Dynamics Laboratory's (GFDL's) ensemble coupled data assimilation v2.0 (www.gfdl.noaa.gov) [*Chang et al.*, 2013] and European Centre for Medium-Range Weather Forecasts' (ECMWF's) ocean reanalysis system 4 (www.ecmwf.int) [*Balmaseda et al.*, 2012]—are used to estimate changes and trends in the depth of the 23°C isotherm (D23) (a proxy for thermocline depth) and upper ocean heat content (OHC). The OHC is calculated as the temperature averaged vertically from the surface to a depth of 100 m [*Price*, 2009]. This method was found to represent the upper ocean energy available for extraction by a TC better than the traditional tropical cyclone heat potential [*Price*, 2009]. Monthly mean sea surface height anomaly data for the period 1981–2010, obtained from NOAA (http://www.esrl.noaa.gov/psd/data/) [*Behringer and Xue*, 2004], was used to compute changes in dynamic sea surface topography.

National Centers for Environmental Prediction (NCEP)-Department of Energy (DOE) Reanalysis 2 [*Kanamitsu et al.*, 2002] monthly mean air temperature, relative humidity, and geopotential height data for the period 1981–2010, obtained from NOAA at http://www.esrl.noaa.gov/psd/data/, are used to calculate changes and trends in moist static energy (MSE) and changes in equivalent potential temperature. The MSE is averaged between the 700 and 925 hPa pressure levels. Corresponding ERA-INTERIM data [*Dee et al.*, 2011] for the same period are also obtained from ECMWF at http://data-portal.ecmwf.int/data/d/interim_moda/ to evaluate changes and trends in MSE. Finally, monthly mean NCEP and ERA-INTERIM 10 m surface wind data are obtained to identify changes in surface circulation, to estimate the surface wind stress, and to calculate the Ekman pumping velocity. For consistency, we focus on results that are based on NCEP atmospheric data and GFDL oceanic data, since NCEP data are used to force the GFDL model. To test the robustness of our results to the data sets used, we repeated the analyses using NOAA SST, ECMWF ocean and ERA-INTERIM atmospheric reanalyses data (see Figures S1 and S2 in the supporting information) and found similar results, suggesting that our conclusions are largely independent of the particular data set chosen (see section S1 in the supporting information).

Following *Yu* [2003], the Ekman pumping velocity (W) is estimated as $W = \frac{1}{\rho f}\left((\nabla \times \tau) + \frac{\beta \tau^x}{f}\right)$. Here ρ is the mean sea water density, τ is the surface wind stress estimated from the 10 m surface wind data, τ^x is the

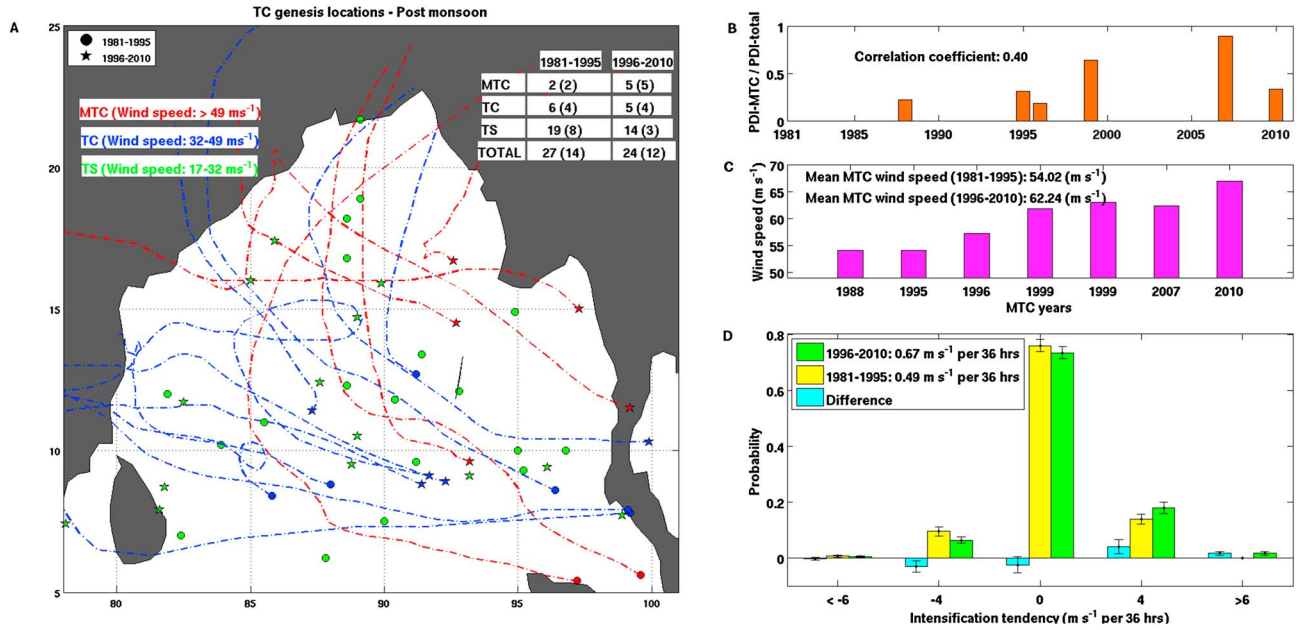

Figure 1. (a) The locations and tracks of storms in the BoB for the period 1981–2010. The number of storms in each category is provided in the table overlaid. The numbers outside the parentheses indicate storm count for the entire BoB, while the numbers inside the parentheses indicate number of storms that formed to the east of 90°E. (b) The ratio between PDI of storms while in major TC-phase (MTC) to the total PDI. The correlation of this ratio with time, indicated in the figure, is statistically significant at the 95% level. (c) Histogram of the mean maximum wind speed during MTC-phase for each MTC. Values of maximum wind speed averaged during MTC-phase for each MTC and over each 15 year period are shown. (d) The PDF of intensification tendencies for the two 15 year periods, 1996–2010 and 1981–1995, and the difference between them, with error bars indicated. For the 1981–1995 period, no bar is shown for the >6 category since there were no storms with an intensification tendency of more than 6 m s^{-1} per 36 h.

zonal component of τ, f is the Coriolis parameter, and β is the meridional gradient of f. We estimate the mean probability distribution function of intensification tendencies and the associated error bars using the Monte Carlo method of random sampling. To test the significance of a change in the storm frequency, we use the statistical Bootstrap technique.

3. Results

The formation locations and numbers of postmonsoon BoB storms for the 30 year period 1981–2010 are shown in Figure 1a and in the table overlaid, respectively. A total of 27 storms formed during the period 1981–1995 compared to 24 storms during 1996–2010. Thus, the two periods are statistically similar in terms of the total storm frequency. During 1981–1995, eight storms achieved TC strength or higher out of a total of 27 storms, for a conversion rate of nearly 30%. On the other hand, 10 out of the 24 total storms attained TC strength or higher between 1996 and 2010, resulting in a higher conversion rate of about 42%. An interesting feature of the BoB TC formation is the zonal asymmetry. Only three out of the 18 TCs formed to the west of 90°E, while an overwhelming 15 TCs formed to the east of 90°E. The difference is much starker for major TCs (MTCs). All seven MTCs that occurred in the BoB formed east of the 90°E longitude. This geographical dependence of TCs can likely be attributed to the longer time spent over the warm ocean for storms that form to the east of 90°E [*Girishkumar and Ravichandran*, 2012].

Next, considering only the storms that formed to the east of 90°E, six out of the 14 storms that formed before 1995 achieved TC strength or higher, while nine out of the 12 storms that formed after 1995 attained a strength of TC or higher, giving conversion rates of 42% and 75% before and after 1995, respectively. Similarly, for MTCs the conversion rates are 14% (two out of 14) and 42% (five out of 12) before and after 1995, respectively. These numbers suggest a stronger tendency for storms to intensify during 1996–2010 compared to the period between 1981 and 1995. But are these changes in conversion rates significant?

Figure 1b shows the time series of the relative contribution of storms while in MTC-phase to the total TC power, which is computed as the ratio between the PDI of storms while in MTC-phase to the total PDI. It is seen that the fraction of power associated with MTC phase increased over the 30 year period and is

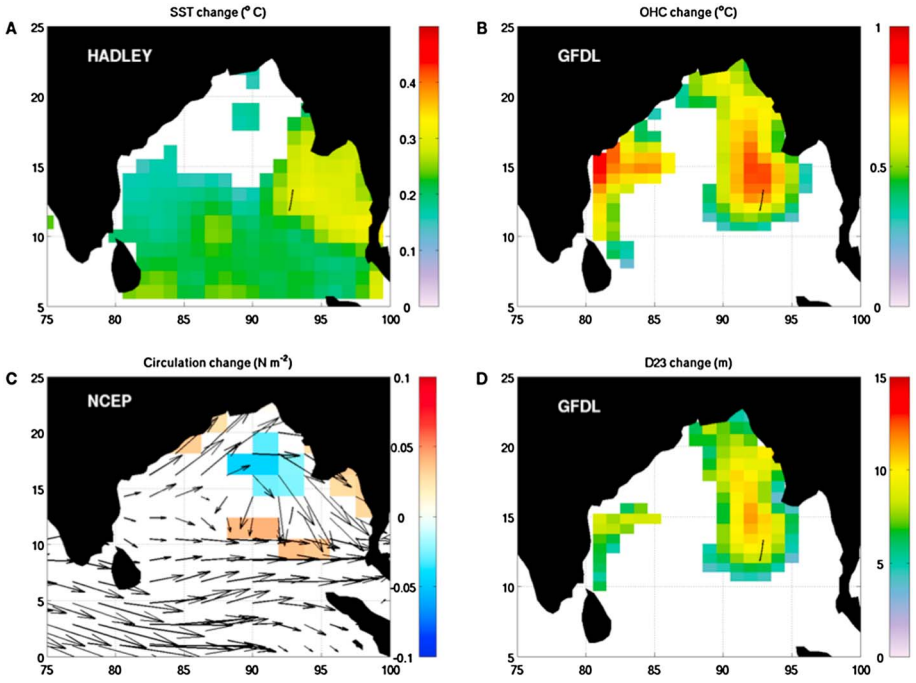

Figure 2. (a) The change in SST based on Hadley SST data. (b) The change in OHC based on GFDL ocean assimilation data. (c) The change in Ekman pumping velocity with changes in surface wind circulation overlaid. (d) The change in thermocline depth (D23) based on GFDL ocean assimilation data. "Change" represents the October–November 1996–2010 mean minus the October–November 1981–1995 mean. All changes shown are statistically significant at the 95% level.

positively correlated with time at 0.40, a value significant at the 95% level. Since the PDI is a metric that combines the storm frequency, duration and intensity into a single parameter that gives an indication of the intensity of the TC season as a whole, changes in any of these parameters could impact the PDI. We noted earlier that the frequency of storms during the two 15 year periods, 1981–1995 and 1996–2010, was statistically identical. Further analysis reveals that the total storm days was nearly the same for the two periods. Also, the mean duration spent by each MTC in MTC-phase during the 15 year period 1996–2010, despite an increase, was statistically indifferent from that during the 15 year period 1981–1995 (see section S2 in the supporting information for details).

Besides storm frequency and longevity, the other factor that can play an important role in its power dissipation is the maximum intensity attained. Figure 1c shows the mean maximum intensity during MTC phase for each of the 7 MTCs. It is seen that the mean maximum intensity sustained by storms during MTC phase has been increasing with time. On average, the maximum wind speed of storms during MTC phase for the period 1981–1995 was about 54 m s^{-1}, which corresponds to category 3. On the other hand, the mean maximum wind speed for storms during MTC phase for the period 1996–2010 was about 62 m s^{-1}, which corresponds to category 4. This difference satisfies the student's *t* test for difference of means at the 95% level. Hence, based on this evidence, the intensity of postmonsoon BoB storms has indeed been increasing.

To further elucidate the difference in storm intensities between the two 15 year periods, the intensification tendency was calculated at each 6-hourly location and the probability density function (PDF) of intensification tendencies was then generated for each 15 year period. Storm locations where the maximum wind speed exceeded 49 m s^{-1} (major TC (MTC) strength) were excluded from our analysis since we are interested in intensification to MTC status. This data subsampling makes the wind speed distributions for the two periods statistically similar, allowing us to make a meaningful comparison of the intensification tendencies between the two periods. The PDFs of intensification tendencies for the two periods and the difference between them, depicted in Figure 1d, show that the PDF for the years 1996–2010 is skewed to the right compared to the PDF for the years 1981–1995. The mean intensification tendency for the period 1981–1995 was 0.49 m s^{-1} 36 h^{-1}, while the mean intensification tendency for the period 1996–2010 was 0.67 m s^{-1} 36 h^{-1}, indicating a 36% increase. This difference between the mean intensification tendencies is statistically

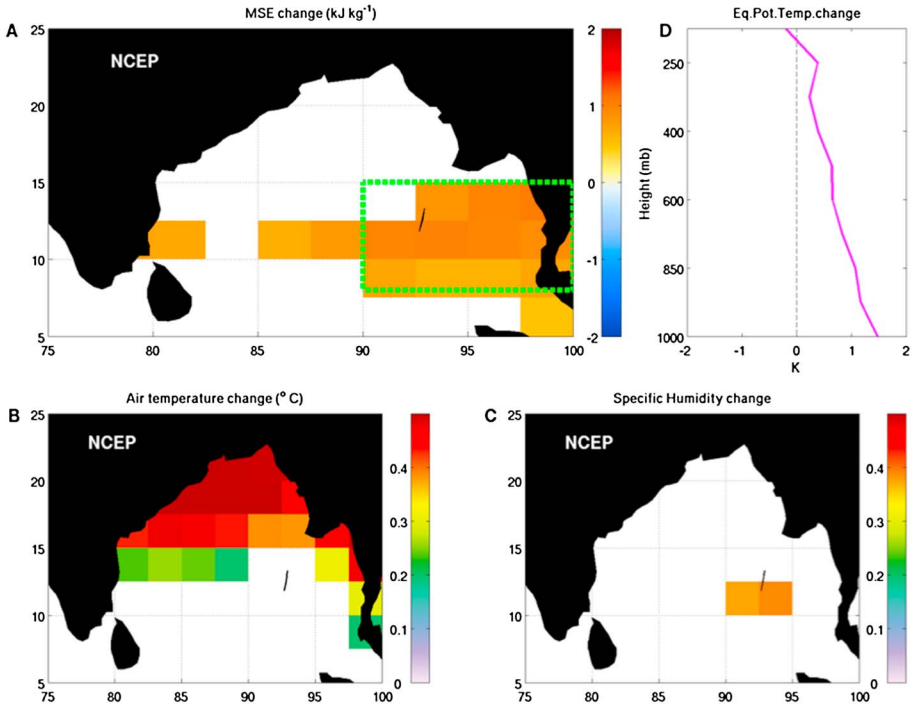

Figure 3. The change in (a) moist static energy (MSE), (b) air temperature, and (c) specific humidity based on NCEP data, each averaged between the 700 and 925 hPA levels. Changes shown are statistically significant at the 95% level. (d) The change in vertical profile of the equivalent potential temperature, averaged over the region enclosed by the green box shown in Figure 3a. Change represents the October–November 1996–2010 mean minus the October–November 1981–1995 mean.

significant at the 90% level, suggesting that the tendency for the storm to intensify rapidly was considerably higher during the latter half of the 30 year period compared to the first half.

The above results lead to the following question: What are the immediate causes for the change in TC activity over the period 1981–2010? Or more simply, can we find corresponding environmental changes as evidence to support the observed change in TC activity? To answer this question, we examine various environmental parameters that play a key role in TC intensification, beginning with those from the ocean. The changes in SST and OHC are shown in Figures 2a and 2b, respectively. Both parameters show increases, suggesting that the ocean became increasingly favorable for TC intensification during the period. Though SST increases almost everywhere south of 15°N and along the coast of Myanmar, the maximum increase is found in the eastern BoB. The strongest SST increase of about 0.3°C occurs approximately in the region between 93°E and 100°E and between 10°N and 17°N. For OHC, the changes are located primarily in two regions. The larger of the two is in the eastern BoB, between 90°E and 95°E and between 10°N and the northern boundary of BoB. The other region of OHC increase occurs along the east coast of India, stretching between 10°N and 20°N. In both regions, the maximum increases of about 0.8–1°C occur at the latitude of 15°N. The OHC represents a combination of the warmth of the upper ocean and the depth to which the warm water extends. SST provides a measure of the warmth of the upper ocean, while the depth of the warm water is related to the thermocline depth (D23). Thus, along with changes in SST, thermocline depth variations also influence OHC.

The D23 in the BoB is chiefly controlled by two mechanisms: local Ekman pumping induced by surface winds and planetary waves generated by surface zonal winds in the equatorial Indian Ocean [*Girishkumar et al.*, 2013]. Considering the changes in surface winds over the BoB (Figure 2c), we find an anomalous anticyclonic circulation feature in the northern Bay, centered near 90°E and 15°N. This circulation feature generated Ekman downwelling in the region between 88°E and 95°E and to the north of 15°N (Figure 2c) and may have contributed to a deepening of D23 over that region during 1996–2010 relative to 1981–1995 (Figure 2d). However, the anticyclonic circulation feature does not explain all of the D23 changes in the BoB. The other notable feature of the change in surface circulation is the enhanced westerly winds in the equatorial Indian

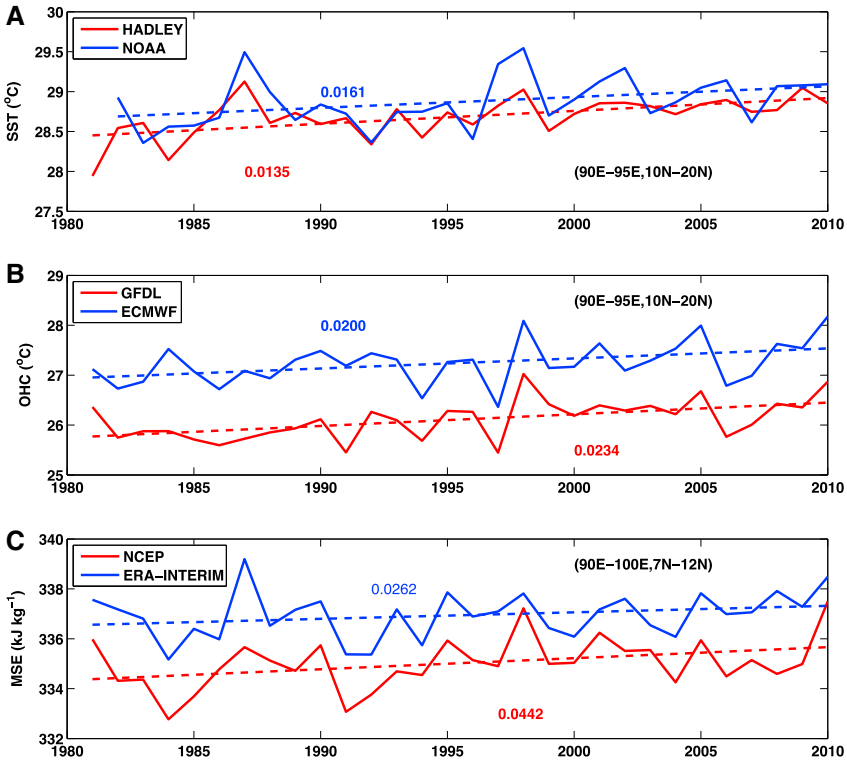

Figure 4. (a) Time series and trends in SST based on Hadley and NOAA data. (b) Time series and trends in OHC based on GFDL and ECMWF ocean reanalyses data. (c) Time series and trends in MSE based on NCEP and ERA-INTERIM atmospheric reanalyses data. The trend values and the area over which each time series was averaged are indicated. All trend values are statistically significant at the 95% level except the MSE trend from ERA-INTERIM, which is significant at the 80% level.

Ocean. Westerly surface winds near the equator (Figure 2c) generate downwelling Kelvin Waves, which after hitting the eastern boundary of Java/Sumatra propagate through the coastal wave guide along the entire rim of the BoB as downwelling coastal Kelvin waves, deepening the thermocline along their path. While at the eastern boundary of the BoB, the Kelvin Waves also radiate westward-propagating Rossby Waves that carry the thermocline signal to the interior of the basin [*Girishkumar et al.*, 2013; *Sreenivas et al.*, 2012]. The propagation of these waves is readily reflected in changes in dynamic sea surface topography (Figure S4). Thus, the enhanced equatorial westerly winds may cause the D23 increase along the east coast of India and reinforce the positive thermocline changes caused by anomalous Ekman pumping in the northeastern BoB.

The above analysis suggests that upper ocean changes in the BoB favored the intensification of TCs more strongly during the second half of the 1981–2010 period. What about the atmosphere? Figure 3a shows the change in the MSE in the lower level atmosphere. The MSE increased primarily in the southeastern BoB in a broad region extending from 90°E to 100°E and between 8°N and 15°N. Since the MSE is a measure of atmospheric instability, the change in MSE suggests that the lower level atmosphere became more convectively unstable during the 15 year period 1996–2010 compared to 1981–1995. To further understand the change in MSE, changes in air temperature and specific humidity were examined. The air temperature increased almost everywhere to the north of 15°N and near the eastern boundary of the BoB in the Andaman Sea (Figure 3b). On the other hand, specific humidity increased over a small region between 90°E and 95°E and between 10°N and 12°N (Figure 3c). Since the change in MSE is centered over the region of significant increase in specific humidity, we conclude that the change in moisture likely dominated the change in air temperature. Additional support for the role of the atmosphere is found in the difference between the mean vertical profiles of the equivalent potential temperature for the two 15 year periods, averaged over the eastern BoB (Figure 3d). The tilting of the profiles suggests an increase in the air-column instability. All the oceanic and atmospheric changes reported above are statistically significant at the 95% level based on a student's *t* test for difference of means. (Changes in vertical wind shear, the other important atmospheric factor that plays a role in TC development, are not statistically significant and hence are not reported.)

4. Discussion

We showed that the intensity of MTCs increased in the BoB between 1981 and 2010. Our analysis of various oceanic and atmospheric parameters indicates that the large-scale environment for TC intensification became more favorable in the eastern BoB for the period 1996–2010 compared to 1981–1995. Since the eastern BoB is where the majority of stronger storms form, it is not surprising that environmental changes in this region would occur simultaneously with a significant increase in the intensity of BoB TCs.

Having established the potential causes for the recent increase in the intensity of postmonsoon BoB storms, it is important to determine if the changes are part of longer-term trends or associated with decadal shifts in the large-scale circulation. Figure 4 shows the time series of SST, OHC, and MSE averaged over the eastern BoB. There are noticeable positive linear trends in the various parameters over the 30 year period. The trend values for SST and OHC are in excellent agreement among different data sets and are statistically significant at the 95% level. For MSE, the trend from NCEP is considerably higher than that from ERA-INTERIM and is significant at the 95% level, while the trend from ERA-INTERIM is significant at the 80% level. Thus, the significant linear trends suggest that the large-scale environment in the eastern BoB may continue to favor TC intensification and that the chance for formation of intense storms may continue to rise in the future. However, the hypothesis that these 30 year trends are representative of long-term secular trends warrants further investigation.

The main conclusions from our study are in general agreement with those from *Elsner et al.* [2008], who show an upward trend in the formation of the strongest TCs in the northern Indian Ocean basin and relate it to global warming-induced rising SSTs. The tropical Indian Ocean exhibits some of the highest SST warming rates observed in the global oceans, and much of this trend can be attributed to anthropogenic climate change [*Knutson et al.*, 2006]. Even during the period of the so-called "hiatus" in global warming, the tropical Indian Ocean SSTs continued to rise [*Luo et al.*, 2012]. Since the low-level moisture and temperature in the atmosphere are strongly dependent on the local SST [*Bhat et al.*, 1996], changes in MSE in the eastern BoB may be related to changes in SST over that region. However, a more careful analysis is required to discern the exact relationship between them.

We showed that the largest increases in SST, OHC, and MSE occurred in the eastern BoB and that the changes in OHC are broadly consistent with increases in SST and thermocline depth. The changes in thermocline depth in turn appear to be related to changes in atmospheric circulation over the BoB and the Northern Indian Ocean. However, the causes of the zonal asymmetry in SST and MSE changes are unclear, as are the mechanisms responsible for the large-scale changes in surface winds. Future studies involving detailed data analysis combined with numerical modeling may unravel the relative contributions of different factors and their potential relationships.

Finally, since major climate phenomena such as the El Niño Southern Oscillation and the Indian Ocean Dipole manifest most strongly during late boreal fall and early winter, they may also influence the postmonsoon BoB TCs [*Girishkumar and Ravichandran*, 2012]. A better understanding of these phenomena may shed more light on the potential role of natural climate variability in the evolution of the postmonsoon BoB TC activity.

Acknowledgments

This research was supported by the Office of Science of the U.S. Department of Energy as part of the Regional and Global Climate Modeling program. The Pacific Northwest National Laboratory is operated for DOE by Battelle Memorial Institute under contract DE-AC05-76RL01830.

The Editor thanks Peter Webster and an anonymous reviewer for their assistance in evaluating this paper.

References

Alam, M., A. Hossain, and S. Shafee (2003), Frequency of Bay of Bengal cyclonic storms and depressions crossing different coastal zones, *Int. J. Climatol.*, *23*, 1119–1125.

Balaguru, K., P. Chang, R. Saravanan, L. R. Leung, Z. Xu, M. Li, and J.-S. Hsieh (2012), Ocean barrier layers effect on tropical cyclone intensification, *Proc. Natl. Acad. Sci.*, *109*(36), 14,343–14,347.

Balmaseda, M. A., K. Mogensen, and A. T. Weaver (2012), Evaluation of the ECMWF ocean reanalysis system ORAS4, *Q. J. R. Meteorol. Soc.*, *139*, 1132–1161.

Behringer, D., and Y. Xue (2004), Evaluation of the global ocean data assimilation system at NCEP: The pacific ocean, in *Proc. Eighth Symp. on Integrated Observing and Assimilation Systems for Atmosphere, Oceans, and Land Surface*, AMS 84th Annual Meeting, Washington State Convention and Trade Center, Seattle, Wash.

Bhat, G., J. Srinivasan, and S. Gadgil (1996), Tropical deep convection, convective available potential energy and sea surface temperature, *J. Meteorol. Soc. Jpn.*, *74*(2), 155–166.

Chang, Y.-S., S. Zhang, A. Rosati, T. L. Delworth, and W. F. Stern (2013), An assessment of oceanic variability for 1960–2010 from the GFDL ensemble coupled data assimilation, *Clim. Dyn.*, *40*(3–4), 775–803.

Dee, D., et al. (2011), The ERA-INTERIM reanalysis: Configuration and performance of the data assimilation system, *Q. J. R. Meteorol. Soc.*, *137*(656), 553–597.

Elsner, J. B., J. P. Kossin, and T. H. Jagger (2008), The increasing intensity of the strongest tropical cyclones, *Nature*, *455*(7209), 92–95.

Emanuel, K. (2005), Increasing destructiveness of tropical cyclones over the past 30 years, *Nature*, *436*(7051), 686–688.
Girishkumar, M., M. Ravichandran, and W. Han (2013), Observed intraseasonal thermocline variability in the Bay of Bengal, *J. Geophys. Res. Oceans*, *118*, 3336–3349, doi:10.1002/jgrc.20245.
Girishkumar, M. S., and M. Ravichandran (2012), The influences of ENSO on tropical cyclone activity in the Bay of Bengal during October–December, *J. Geophys. Res.*, *117*, C02033, doi:10.1029/2011JC007417.
Hoarau, K., J. Bernard, and L. Chalonge (2012), Intense tropical cyclone activities in the northern Indian ocean, *Int. J. Climatol.*, *32*(13), 1935–1945.
Islam, T., and R. E. Peterson (2009), Climatology of landfalling tropical cyclones in Bangladesh 1877–2003, *Nat. Hazard.*, *48*(1), 115–135.
Kanamitsu, M., W. Ebisuzaki, J. Woollen, S.-K. Yang, J. Hnilo, M. Fiorino, and G. Potter (2002), NCEP-DOE AMIP-II Reanalysis (R–2), *Bull. Am. Meteorol. Soc.*, *83*(11), 1631–1643.
Kikuchi, K., and B. Wang (2010), Formation of tropical cyclones in the northern indian ocean associated with two types of tropical intraseasonal oscillation modes, *J. Meteorol. Soc. Jpn.*, *88*(3), 475–496.
Klotzbach, P. J. (2006), Trends in global tropical cyclone activity over the past twenty years (1986–2005), *Geophys. Res. Lett.*, *33*, L10805, doi:10.1029/2006GL025881.
Knutson, T. R., and R. E. Tuleya (2004), Impact of CO_2-induced warming on simulated hurricane intensity and precipitation: Sensitivity to the choice of climate model and convective parameterization, *J. Clim.*, *17*(18), 3477–3495.
Knutson, T. R., T. Delworth, K. Dixon, I. Held, J. Lu, V. Ramaswamy, M. Schwarzkopf, G. Stenchikov, and R. Stouffer (2006), Assessment of twentieth-century regional surface temperature trends using the GFDL CM2 coupled models, *J. Clim.*, *19*(9), 1624–1651.
Lin, I.-I., C.-H. Chen, I.-F. Pun, W. T. Liu, and C.-C. Wu (2009), Warm ocean anomaly, air sea fluxes, and the rapid intensification of Tropical Cyclone Nargis, 2008, *Geophys. Res. Lett.*, *36*, L03817, doi:10.1029/2008GL035815.
Lloyd, I. D., and G. A. Vecchi (2011), Observational evidence for oceanic controls on hurricane intensity, *J. Clim.*, *24*(4), 1138–1153.
Luo, J.-J., W. Sasaki, and Y. Masumoto (2012), Indian ocean warming modulates pacific climate change, *Proc. Natl. Acad. Sci.*, *109*(46), 18,701–18,706.
McPhaden, M. J., G. R. Foltz, T. Lee, V. Murty, M. Ravichandran, G. A. Vecchi, J. Vialard, J. D. Wiggert, and L. Yu (2009), Ocean-atmosphere interactions during cyclone nargis, *Eos, Trans. AGU*, *90*(7), 53–54, doi:10.1029/2009EO070001.
Ng, E. K., and J. C. Chan (2012), Interannual variations of tropical cyclone activity over the north Indian Ocean, *Int. J. Climatol.*, *32*(6), 819–830.
Price, J. F. (2009), Metrics of hurricane-ocean interaction: Vertically-integrated or vertically-averaged ocean temperature?, *Ocean Sci. Discuss.*, *6*(2), 909–951.
Rayner, N., D. Parker, E. Horton, C. Folland, L. Alexander, D. Rowell, E. Kent, and A. Kaplan (2003), Global analyses of sea surface temperature, sea ice, and night marine air temperature since the late nineteenth century, *J. Geophys. Res.*, *108*(D14), 4407, doi:10.1029/2002JD002670.
Reynolds, R. W., N. A. Rayner, T. M. Smith, D. C. Stokes, and W. Wang (2002), An improved in situ and satellite SST analysis for climate, *J. Clim.*, *15*(13), 1609–1625.
Sengupta, D., B. R. Goddalehundi, and D. Anitha (2008), Cyclone-induced mixing does not cool SST in the post-monsoon north Bay of Bengal, *Atmos. Sci. Lett.*, *9*(1), 1–6.
Singh, O., T. M. A. Khan, and M. S. Rahman (2001), Has the frequency of intense tropical cyclones increased in the north Indian Ocean?, *Curr. Sci.*, *80*(4), 575–580.
Singh, O. P. (2008), Indian Ocean dipole mode and tropical cyclone frequency, *Curr. Sci.*, *94*(1), 29–31.
Sprintall, J., and M. Tomczak (1992), Evidence of the barrier layer in the surface layer of the tropics, *J. Geophys. Res.*, *97*(C5), 7305–7316.
Sreenivas, P., C. Gnanaseelan, and K. Prasad (2012), Influence of El Niño and Indian Ocean dipole on sea level variability in the Bay of Bengal, *Global Planet. Change*, *80*, 215–225.
Webster, P. J. (2008), Myanmar's deadly daffodil, *Nat. Geosci.*, *1*(8), 488–490.
Webster, P. J., G. J. Holland, J. A. Curry, and H.-R. Chang (2005), Changes in tropical cyclone number, duration, and intensity in a warming environment, *Science*, *309*(5742), 1844–1846.
Yu, L. (2003), Variability of the depth of the 20 c isotherm along 6 n in the bay of bengal: Its response to remote and local forcing and its relation to satellite SSH variability, *Deep Sea Res. Part II*, *50*(12), 2285–2304.